

# The GERDA Experiment for the Search of Neutrinoless Double Beta Decay

*Manuel Walter for the GERDA collaboration*

Physik-Institut, Universität Zürich, 8057 Zürich, Switzerland

**DOI:** will be assigned

The GERDA experiment, situated at Laboratori Nazionali del Gran Sasso is designed to search for the neutrinoless double  $\beta$  decay. Bare high purity Ge-diodes enriched to 86% in  $^{76}\text{Ge}$  are directly immersed into liquid Ar. Phase I operated from November 2011 till May 2013 yielding an exposure of 21.6 kg·yr, with a mean background near the Q-value of  $2 \cdot 10^{-2}$  cts/(keV·kg·yr). A half-life of  $1.84_{+0.14}^{-0.10} \cdot 10^{21}$  yr was recently published for the two-neutrino double  $\beta$  decay. For Phase II, additional 20 kg of broad-energy Ge detectors will be installed to reach an exposure of 100 kg·yr with one order of magnitude less background, exploring half-lives up to  $1.5 \cdot 10^{26}$  yr. This will be achieved by liquid Ar instrumentation as an active veto, pulse shape analysis and a refined selection of radio-pure materials.

## 1 Introduction

For some even-even nuclei single  $\beta$ -decay is energetically forbidden, but the neutrino accompanied double  $\beta$  decay ( $2\nu\beta\beta$ ) is allowed. This standard model process has been observed for  $^{48}\text{Ca}$ ,  $^{76}\text{Ge}$ ,  $^{82}\text{Se}$ ,  $^{96}\text{Zr}$ ,  $^{100}\text{Mo}$ ,  $^{116}\text{Cd}$ ,  $^{128}\text{Te}$ ,  $^{130}\text{Te}$ ,  $^{150}\text{Nd}$ ,  $^{238}\text{U}$ ,  $^{130}\text{Ba}$  and  $^{136}\text{Xe}$  with a half-life between  $7 \cdot 10^{18}$  yr and  $2.5 \cdot 10^{24}$  yr. For  $^{76}\text{Ge}$  it has been measure in GERDA to be  $1.84_{-0.10}^{+0.14} \cdot 10^{21}$  yr [1].

The neutrinoless double  $\beta$  decay ( $0\nu\beta\beta$ ) is not allowed in the standard model, it is however predicted by several extensions of the standard model. The most likely mechanism is by the exchange of light neutrinos. The existence of this decay in  $^{76}\text{Ge}$  has been claimed by a subgroup of the Heidelberg-Moscow-Experiment [2].

The double  $\beta$  decay is detected by the summed energy of the two emitted electrons. In the neutrino accompanied decay, part of the energy is carried away by the neutrinos resulting in a continuous spectrum. For the neutrinoless case the energy is carried by the electrons only, resulting in a peak at the Q-value of the decay ( $Q_{\beta\beta} = 2039$  keV for  $^{76}\text{Ge}$ ). In GERDA, Ge is used as both the decay source and the detection device. Ge detectors have a very high energy resolution, around 0.14% at 2 MeV, which is important as a higher resolution results in a larger signal-to-background ratio.

## 2 The Low Background Experiment GERDA

GERDA is running in two phases. Phase I started in November 2011 and finished in May 2013 with 18 kg of enriched Ge diodes. Phase II is planned to start end of 2013 with additional 20 kg of enriched Ge and a background reduced by a factor of 10 compared to Phase I.

In GERDA bare Ge diodes enriched to 86% of  $^{76}\text{Ge}$  are directly immersed into a 5.5 m high cryostat containing  $64\text{m}^3$  of liquid Ar. The Ar serves as a coolant at 89 K and shielding. The cryostat is surrounded by a high purity water tank acting as additional shielding. It is equipped with photomultiplier tubes to veto muon induced events by their Cherenkov light emitted when passing through the water. Muons flying through the neck of the cryostat are detected by plastic scintillator panels installed above the water tank. For a detailed description of the GERDA experiment see [3].

### 2.1 Phase I

One non-enriched and eight refurbished enriched coaxial detectors from the past IGEX and Heidelberg-Moscow experiments were installed in Phase I. The latter are the same as used for the claimed observation. Two of the enriched detectors quickly developed high leakage currents and could not be used for the analysis. Additionally, five Phase II type Broad Energy Germanium (BEGe) detectors were installed in July 2012 of which one showed drifts in the energy calibration and was not used.

Coaxial and BEGe detectors differ by their geometry. Both types have the n-doped electrode on their outer surface shown in black in Fig. 1. The p-doped readout electrode is a pad on one face for the BEGe type detectors and a hole in the center for coaxial type detectors. For more details see section 2.2.1.

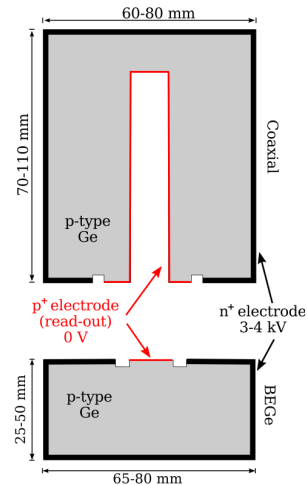


Figure 1: Cut through the rotation symmetry axis of coaxial and BEGe type detectors. Figure from [5].

#### 2.1.1 Data Taking and Detector Stability

A total exposure of enriched Ge detectors of  $21.6\text{ kg}\cdot\text{yr}$  was reached during Phase I [4]. The data was taken with a blinded energy window of  $Q_{\beta\beta} \pm 20\text{ keV}$ . The open part of the data was used to develop analysis methods and background models. The unblinding was performed in two steps, first the blinding window was reduced to  $Q_{\beta\beta} \pm 5\text{ keV}$  for coaxial and  $Q_{\beta\beta} \pm 4\text{ keV}$  for BEGe detectors. The now unblind “side bands” were used to test the background models. Then the full energy range was unblinded and the unchanged analysis methods were applied.

For energy calibration of the Ge detectors about 10 peaks from a  $^{228}\text{Th}$  source were used. The number of peaks used depends on the statistics in the individual peaks for each detector and calibration measurement. The FWHM at  $2614.5\text{ keV}$  was between  $4.2$  and  $5.8\text{ keV}$  for coaxial and between  $2.6$  and  $4.0\text{ keV}$  for BEGe detectors. The maximum shift of this peak between two consecutive calibration measurements was about  $2\text{ keV}$  [5].

#### 2.1.2 Description of Background Sources

Several sources contributing to the background near  $Q_{\beta\beta}$  are known and illustrated in Fig. 2. To understand those it is essential to know that the outer most, so called dead layer of the detector is not active. Interactions in this region will result in no signal. This layer is about 2mm at the n+ contact and about  $0.3\ \mu\text{m}$  for the p+ contact. Electrons from  $\beta$  decays can penetrate either layer whereas  $\alpha$  particles are able to penetrate only the p+ dead layer. There is a transition layer with incomplete charge collection between the active and dead volume.

High energy  $\beta$  decays contributing to the background in GERDA near  $Q_{\beta\beta}$  originate primarily from  $^{42}\text{K}$  in liquid Ar close to the detector surface and  $^{214}\text{Bi}$  on the p+ contact.  $^{42}\text{K}$  is the daughter of  $^{42}\text{Ar}$ , traces of which are naturally contained in Ar. The background from  $^{42}\text{K}$  is approximately a factor of 10 higher than expected.  $^{214}\text{Bi}$  originates from  $^{226}\text{Ra}$  present on the detector surface. Cosmogenically produced  $^{60}\text{Co}$  is an internal  $\beta$  emitter occurring in coincidence with the emission of  $\gamma$  rays.  $\alpha$  events originate from  $^{210}\text{Po}$  and  $^{226}\text{Ra}$ , including its daughter nuclei, on the p+ surface.  $^{222}\text{Rn}$  is also present in liquid Ar near by [5].

Many materials and hence various set-up components contain elements from the  $^{238}\text{U}$  and  $^{232}\text{Th}$  decay chains. Among those the isotopes  $^{208}\text{Tl}$  and  $^{214}\text{Bi}$  emit  $\gamma$  rays which contribute to the background at  $Q_{\beta\beta}$  by Compton scattering. This is also the case for cosmogenic  $^{60}\text{Co}$ . These type of events can have several interaction locations inside the active volume, in which case they are called multi site events. Events with only one interaction location, like most double  $\beta$  decay events, are called single site events. The number of multi site events is reduced by cutting detector coincidences and using pulse shape analysis. The latter is described in [7]. The number of surface  $\beta$  events were reduced using thin copper cylinders, so called mini-shrouds, preventing  $^{42}\text{K}$  ions from drifting to the detector surface. A larger copper cylinder called radon shroud is installed with the goal to prevent Rn emanated from the cryostat from reaching the detector assembly.

### 2.1.3 Background Analysis

The coaxial detectors account for the largest fraction of the total Phase I exposure. For this reason the description of the background is focused on those detectors.

In a first step the spectral shape of each individual background source was simulated. A source is a sub decay chain expected to be in equilibrium and in a specific location in GERDA, e.g. the detector holders, p+ contact, etc.. A minimum number of well motivated sources resulting in a good fit of the measured spectrum are contained in the so called minimum model. These are all sources described in chapter 2.1.2 plus the  $2\nu\beta\beta$  decay and  $^{40}\text{K}$ . The measured spectrum, the model fit and the contributions of its individual components are shown in Fig. 3.

Alpha events clearly dominate the high energy region having a long tail on the low energy side. The tail of  $\alpha$  events originates from different track length inside the dead- and transition layer as well as in liquid Ar, which means different amounts of not detected energy deposition. The contribution due to  $\alpha$  events is extending down to energies below  $Q_{\beta\beta}$ . A zoom to the energy region around  $Q_{\beta\beta}$  is shown in Fig. 4 on the left side. The main contributions at  $Q_{\beta\beta}$

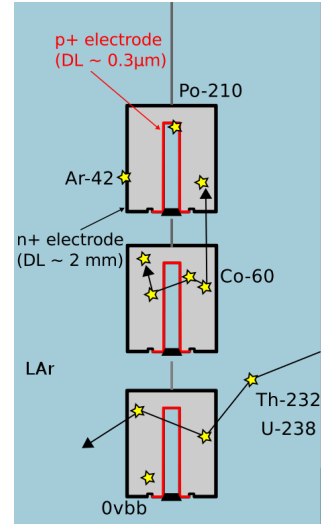


Figure 2: Illustration of typical interaction patterns for different background sources. Figure from [6].

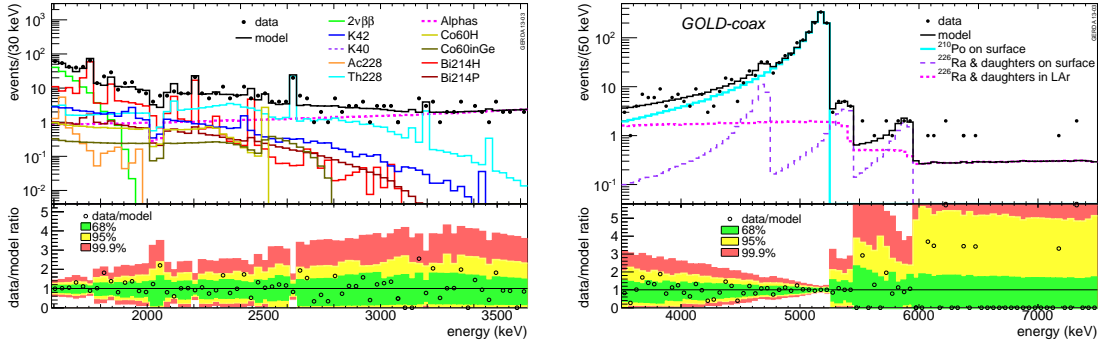


Figure 3: Fit of the minimal model to the measured spectrum in the enriched coaxial detectors and the individual components. Bottom part: Data divided by model with 68% (green), 95% (yellow) and 99.9% (red) probability intervals obtained from the model. Figure from [5].

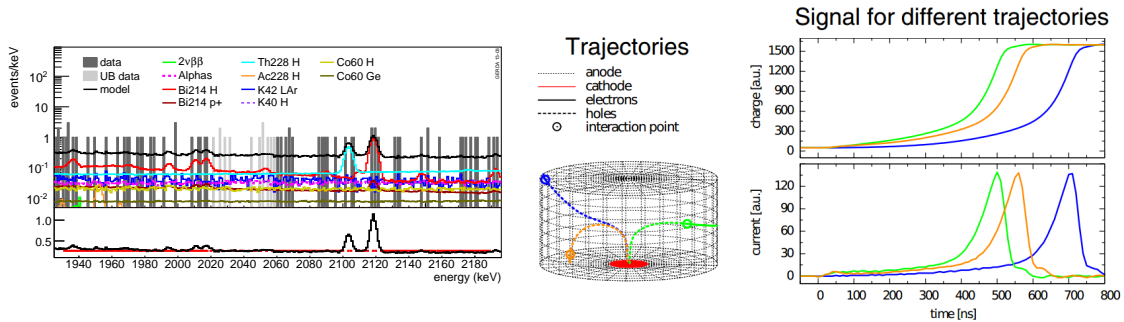


Figure 4: Left: Zoom into the energy region near  $Q_{\beta\beta}$  together with the observed events, the minimum model and its individual components. A comparison of a constant fit and the model is shown in the lower half. A BEGe detector is shown in the center with three interactions (circles) and the resulting drift paths of the excited electrons and holes. Right and center from [8].

are in descending order  $^{214}\text{Bi}$  and  $^{228}\text{Th}$  from detector holders or other close objects,  $^{42}\text{K}$  in liquid Ar and  $\alpha$  decays close to the p+ surface.

Additionally to the sources in the minimum model,  $^{42}\text{K}$  on the p+ and n+ surfaces of the detectors,  $^{228}\text{Th}$  on the radon shroud and on the heat exchanger,  $^{228}\text{Ac}$  and  $^{214}\text{Bi}$  on the radon shroud and  $^{214}\text{Bi}$  in liquid Ar close to p+ surface of the detectors are contained in a maximum model. The main difference is a higher contribution from surface and close to surface events compared to the minimum model.

From both models we do not expect a background peak at  $Q_{\beta\beta}$ . A constant fit to the background excluding the blinded region and  $\pm 5\text{keV}$  around the  $\gamma$  lines at 2104 keV ( $^{208}\text{Tl}$  single escape line) and 2119 keV ( $^{214}\text{Bi}$ ) describes the background at  $Q_{\beta\beta}$  well. This is shown at the bottom left part in Fig. 4. The predicted background from the two models is between  $1.76 \cdot 10^{-2}$  and  $2.38 \cdot 10^{-2} \text{cts}/(\text{keV} \cdot \text{kg} \cdot \text{yr})$ . This is consistent with an extrapolation from a constant background. Shown in gray are the events in the unblinded sidebands which have not been used in

the fits. They match well with the expectations from both models.

In the energy range above the endpoint of  $^{39}\text{Ar}$  at 565 keV till about 1650 keV the  $2\nu\beta\beta$  decay is dominating the spectrum. Both background models provide a half-life for this decay consistent with our previously published value of  $1.84_{-0.10}^{+0.14} \cdot 10^{21}$  yr [1]. For more details about the background in GERDA see [5].

## 2.2 Phase II

In Phase II the mass of enriched Ge will be increased by 20 kg and the background will be reduced by a factor of 10. The latter will be achieved primarily by an active liquid Ar veto system and enhanced pulse shape discrimination properties of the BEGe type Phase II detectors.

### 2.2.1 Broad Energy Ge Detectors

The specific geometry of BEGe detectors, as described in chapter 2.1 results in well separated current peaks for different interaction locations of  $\gamma$  rays inside the detector [8]. Three interaction points (circles) together with the trajectories of the corresponding excited electrons (solid lines) and holes (dashed lines) are shown in the center of Fig. 4. On the right the corresponding charge and current pulses are shown (for a normalized energy deposition at each interaction point). A current signal from a single site,  $\beta\beta$  like event has only one maximum, whereas a multi site, background like event is the sum of several current signals resulting in two or more maxima. This provides the possibility to effectively reject multi site events.

Events with an energy deposition in the transition layer have a different rise time compared to bulk events. This gives the possibility to reject  $\alpha$  and  $\beta$  particles penetrating the dead layer.

An other advantage of BEGe type detectors is their low capacitance compared to coaxial detectors which results in a typical energy resolution of 2.7 keV instead of 4.5 keV FWHM at  $Q_{\beta\beta}$ .

### 2.2.2 Liquid Argon Veto

Many background events at  $Q_{\beta\beta}$  occur in coincidence with an energy deposition in liquid Ar. Ar is a scintillator and hence can be used to efficiently suppress these background events. Suppression factors of a liquid Ar veto system have been measured in a test set-up for different sources. For close sources like impurities in holders, pre-amplifiers and other close objects suppression factors are approximately 1180 for  $^{208}\text{Tl}$  in the  $^{228}\text{Th}$  chain and approximately 4.6 for  $^{214}\text{Bi}$ . The large suppression factor of the former originates from coincident  $\gamma$  decays.

Ar scintillation light has a wavelength of 128 nm and needs to be converted to longer wavelength before detection. In GERDA the conversion is performed by tetraphenyl butadiene coated Tetratex® reflector foils and wavelength shifting fibers. The design of the veto system is shown in Fig. 5. It consists of three cylinders which are called shrouds and a



Figure 5: Schematic view of the liquid Ar veto system. Figure by courtesy of M. Heisel, MPI-K.

PMT array at the top and bottom. The middle shroud, surrounding the Ge-detector strings consists of a close array of approximately 1000 m of fibers with Si photomultipliers at the end. This allows light from outside the shroud to be detected. The upper and lower shroud is made of Cu covered from the inside by the coated Tetratex® reflector.

### 3 Conclusions

Phase I of the GERDA experiment has successfully finished with an exposure of 21.6 kg·yr and a background of about  $2 \cdot 10^{-2}$  cts/(keV·kg·yr). A detailed analysis shows that no peak from the background is expected at  $Q_{\beta\beta}$ . The results of Phase I have been published [4] soon after the Patras 2013 workshop. The transition to Phase II with a design sensitivity improvement by a factor of 10 has started.

### 4 Acknowledgments

The GERDA experiment is supported financially by the German Federal Ministry for Education and Research (BMBF), the German Research Foundation (DFG) via the Excellence Cluster Universe, the Italian Istituto Nazionale di Fisica Nucleare (INFN), the Max Planck Society (MPG), the Polish National Science Centre (NCN), the Foundation for Polish Science (MPD programme), the Russian Foundation for Basic Research (RFBR 12- 02-12135-ofi-M), and the Swiss National Science Foundation (SNF). The institutions acknowledge also internal financial support.

The GERDA collaboration thanks the directors and the staff of the LNGS for their continuous strong support of the GERDA experiment.

### 5 Bibliography

#### References

- [1] GERDA collaboration, “Measurement of the half-life of the two-neutrino double beta decay of Ge-76 with the GERDA experiment”, *J. Phys. G: Nucl. Part. Phys.* **40** (2013) 035110 [arXiv:1212.3210 [nucl-ex]]
- [2] H.V. Klapdor-Kleingrothaus, I.V. Krivosheina, A. Dietz, O. Chkvorets, “Search for neutrinoless double beta decay with enriched  $^{76}\text{Ge}$  in Gran Sasso 1990–2003”, *Phys. Lett.* **B586**, 198 (2004) [arXiv:hep-ph/0404088]
- [3] GERDA collaboration, “The GERDA experiment for the search of  $0\nu\beta\beta$  decay in  $^{76}\text{Ge}$ ”, *Eur. Phys. J. C* **73** (2013) 2330 [arXiv:1212.4067 [physics.ins-det]]
- [4] GERDA collaboration, “Results on neutrinoless double beta decay of  $^{76}\text{Ge}$  from GERDA Phase I”, *Phys. Rev. Lett.* **111**, 122503 (2013), [arXiv:1307.4720 [nucl-ex]]
- [5] GERDA collaboration, “The background in the  $0\nu\beta\beta$  experiment GERDA”, submitted to *Eur. Phys. J. C* [arXiv:1306.5084v1 [physics.ins-det]]
- [6] M. Agostini, “The GERDA experiment for the search of neutrinoless double beta decay: status and perspectives” talk at 25th Rencontres de Blois, May 26-31, 2013
- [7] GERDA collaboration, “Pulse shape discrimination for GERDA Phase I data”, submitted to *Eur. Phys. J. C* [arXiv:1307.2610v1 [physics.ins-det]]
- [8] M. Agostini, C. A. Ur, D. Budjas, E. Bellotti, R. Brugnera, C. M. Cattadori, A. di Vacri, A. Garfagnini, L. Pandola and S. Schönert, “Signal modeling of high-purity Ge detectors with a small read-out electrode and application to neutrinoless double beta decay search in Ge-76” *J. of Instrumentation (JINST)*, **6** (2011) P03005 [arXiv:1012.4300 [physics.ins-det]]